THE JOURNAL OF PHYSICAL CHEMISTRY LETTERS
A JOURNAL OF THE AMERICAN CHEMICAL SOCIETY

pubs.acs.org/JPCL

Letter

Ultrafast Transient Electroabsorption Illuminates Additive Effects for Enhancing Non-fullerene Photovoltaic Devices

Aditi Kumar, Bo-Han Chen,* Chao-Yang Lin, Nikita A. Shumilov, Nathaniel J. L. K. Davis, Yu-Chiang Chao, Li-Kang Chu, Chia-Feng Li, Yu-Ching Huang, Shang-Da Yang, Michael B. Price, Paul A. Hume,* Justin M. Hodgkiss,* and Kai Chen*

Cite This: *J. Phys. Chem. Lett.* 2025, 16, 10703−10711

Read Online

ACCESS | Metrics & More | Article Recommendations | Supporting Information

ABSTRACT: Additives are crucial in optimizing organic photovoltaic (OPV) performance, yet their influence on intrinsic photophysical properties remains underexplored. Here we use sub-55 fs transient absorption spectroscopy to extract the transient electroabsorption (TEA) response—a sensitive and contactless probe of electronic coupling—in Y6 films processed with 0.5% 1,8-diiodooctane (DIO) or 1-chloronaphthalene (CN). The DIO-treated film exhibits a primarily first-derivative-like signal, whereas the CN-treated film displays a second-derivative-like response, indicating enhanced delocalized charge transfer character and stronger core−core interactions. Additionally, the TEA rise time in CN-treated films is an order of magnitude shorter than in DIO-treated ones (0.2 ps vs 2 ps). Importantly, these TEA dynamics quantitatively mirror charge generation rates in PM6:Y6 blends, establishing TEA as a predictive metric of OPV performance. Our results uncover a direct nanomorphology−dynamics−function relationship and offer a powerful framework for rational additive design and selection in next-generation OPVs.

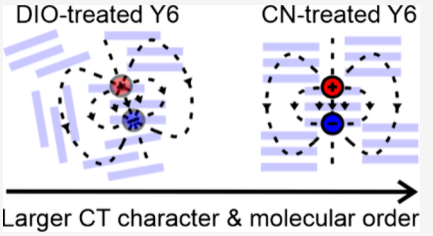

The synthesis of the non-fullerene acceptor Y6 with an A−DA′D−A molecular structure incorporating an electron-deficient A′ unit within the electron-rich donor backbone in 2019 marked a significant milestone in the field of organic photovoltaics (OPVs), leading to a notable increase in power conversion efficiency from 12.1% to 15.6%.[1] Since then, extensive research has been conducted to elucidate the structure−function relationship of Y6 and its derivatives, enhancing the efficiency of OPV devices incorporating them.[2−7] Among these efforts, additive engineering has emerged as a particularly effective strategy for optimizing device performance.[8−11]

The PM6:Y6 bulk heterojunction (BHJ) has been extensively studied, with over 2230 publications.[12] A recent comprehensive review of these studies identified the conjugated 1-chloronaphthalene (CN) as the most frequently utilized additive in this high-performing system.[1,9,11−15] Grazing incidence wide-angle X-ray scattering (GIWAXS) has shown that 0.5% CN additive facilitates more ordered molecular packing of Y6 within the BHJ, whereas the linear aliphatic additive 1,8-diiodooctane (DIO) induces random Y6 orientations.[9] It was suggested that the disorder induced by DIO increases energetic heterogeneity, narrows the active layer bandgap, and sharply reduces the open circuit voltage (V_{oc}) of the device.[9] All-atom molecular dynamics (MD) simulations showed that both additives preferentially interact with Y6 rather than PM6, explaining the lack of impact on the PM6 phase observed in time-resolved in situ UV−vis absorption measurements.[9,11] Additionally, grazing transmission small-angle X-ray scattering suggests that CN and DIO do not alter the crystallinity of PM6 nor the nanoscale phase separation in PM6:Y6 BHJs, reinforcing the role of Y6 molecular packing as the key reason for the performance differences. Notably, even at PM6:Y6 ratios of 1:2 or 1:4 with CN as an additive, all key device parameters remain stable, emphasizing the importance of Y6 ordering in achieving high efficiencies.[9]

Since PM6 remains largely unaffected by additives and Y6 maintains its crystalline packing when transitioning from neat films to the BHJ,[5] here we focus on the impact of additives on neat Y6 thin films. MD simulations have demonstrated that π-interactions between CN and the IC-2F end groups of Y6 play a crucial role in long-range molecular ordering and enhancing the packing density in this film.[9] The same study also showed that, although all films (as-cast and additive-treated) primarily (∼50%) adopt tail−tail dimer configurations (Supporting Information (SI) section 3), the presence of DIO markedly suppresses core−core (cofacial) dimer formation. These findings were further corroborated by an independent all-atom MD study, which demonstrated that conjugated additives such as CN reduce intermolecular distances and strengthen

Received: August 26, 2025
Revised: September 22, 2025
Accepted: September 23, 2025
Published: October 6, 2025

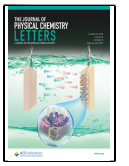

https://doi.org/10.1021/acs.jpclett.5c02643
J. Phys. Chem. Lett. 2025, 16, 10703−10711

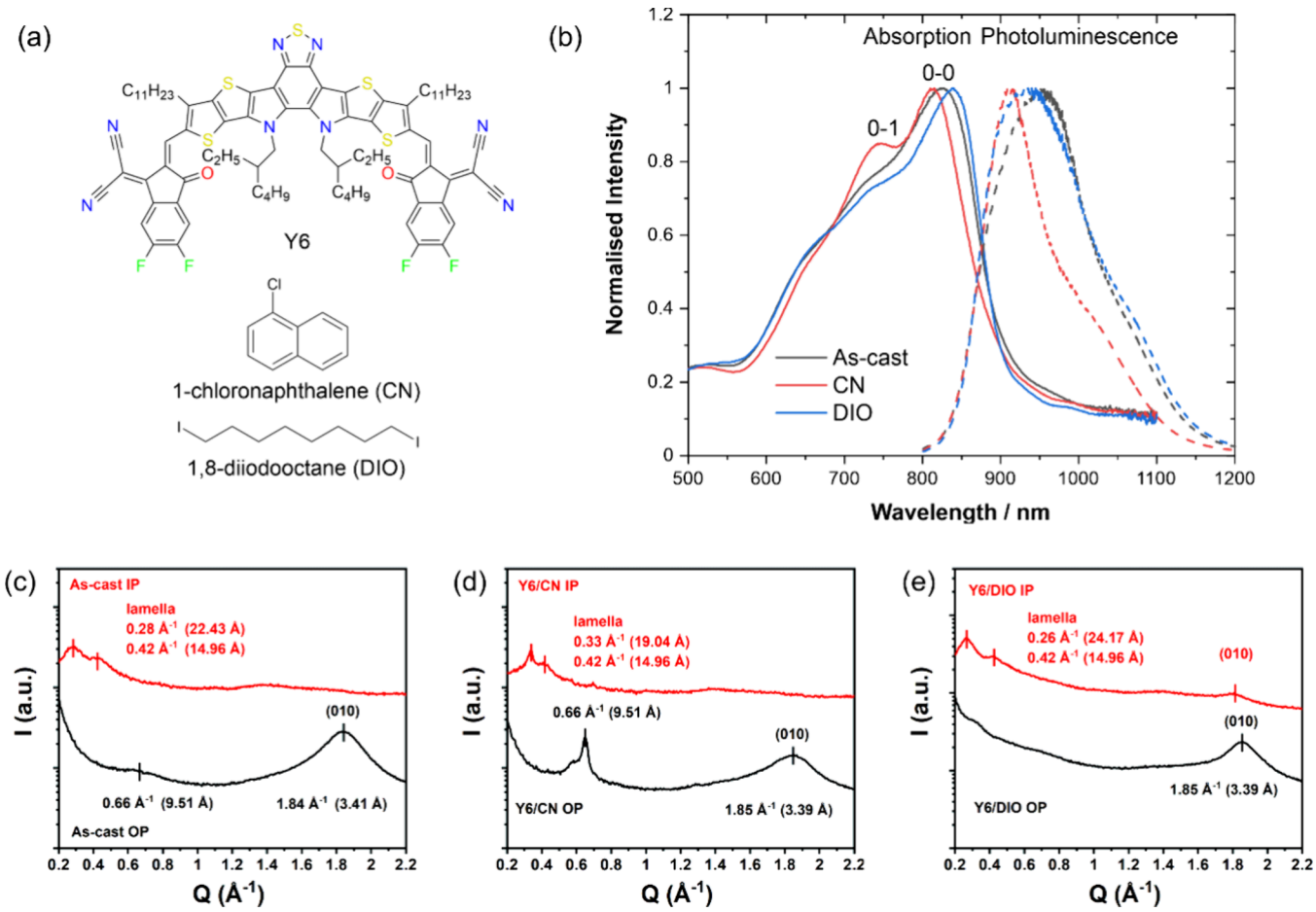

Figure 1. (a) Molecular structures of Y6, 1-chloronaphthalene (CN), and 1,8-diiodooctane (DIO). (b) Normalized absorption (solid lines) and photoluminescence (dashed lines) spectra of the three films: as-cast Y6 in chloroform in black, 0.5% CN additive with 80 °C thermal annealing in red, and 0.5% DIO additive with 80 °C thermal annealing in blue. (c−e) GIWAXS line cuts for the (c) as-cast (d) CN-treated, and (e) DIO-treated thin films. The red line cuts present the in-plane (IP) direction, and the black line cuts present the out-of-plane (OP) direction.

core−core interactions relative to nonconjugated additives like DIO.[16]

While the structural changes associated with additives are largely understood, the influence of packing on electronic interactions within the neat film remains less explored. In this context, electroabsorption (EA) spectroscopy serves as a powerful tool for investigating the electronic properties of materials by analyzing variations in their absorption spectrum under an applied electric field.[17−20] EA measurements are typically conducted through two approaches: steady-state EA on devices, and transient electroabsorption (TEA) signatures observed in transient absorption (TA) data. In steady-state EA, an external electric field is applied to a material, inducing shifts and splitting in electronic energy levels via the Stark effect.[21] In contrast, TEA signals in TA measurements arise from the formation of intermolecular charge-transfer (CT) states, which generate local electric fields that modulate the absorption spectrum of neighboring molecules.[22,23] According to the Stark effect, the energy of an electronic state is altered by an electric field − whether externally applied or internally generated − depending on its polarizability (p) and dipole moment (μ).[17,18]

In organic materials, the low dielectric constant leads to the formation of strongly bound Frenkel excitons, which primarily exhibit neutral local excitonic character.[24] This influences the material's polarizability and modifies the arrangement of the electron cloud, resulting in EA spectral line shapes that resemble the first derivative of the absorption spectrum.[25,26] Interestingly, recent steady-state EA studies have revealed that Y6 exhibits a predominantly second derivative EA response in both neat films[24] and blends.[27] A second derivative line shape is associated with changes in dipole moment upon excitation and reflects increased electron−hole separation in the excited state, providing insight into the extent of charge transfer character.[21,28,29] This behavior contrasts sharply with that of the linear A−D−A non-fullerene acceptor ITIC, which primarily exhibits a first derivative EA response.[24,30]

Ultrafast spectroscopy studies have consistently detected the emergence of TEA signals in Y-type acceptors on subpicosecond time scales, originating from the conversion/migration of local excitons (LE) generated in amorphous regions of the film to intermolecular CT states in densely packed regions of the film.[23] Notably, the TEA spectral shape closely matches that of the steady-state EA seen in device measurements, making TEA a valuable tool for tracking LE to intermolecular CT state migration kinetics. Furthermore, steric hindrance and reduced intermolecular interaction strength have been shown to accelerate the migration of the LE to intermolecular CT states in well packed regions of the film. For instance, Y6 exhibits a LE-to-intermolecular CT transfer time of ∼2.9 ps, significantly slower than the ∼1.0 ps transfer time observed for the more sterically hindered L8-BO.[23] In our previous work,[31]

https://doi.org/10.1021/acs.jpclett.5c02643
J. Phys. Chem. Lett. 2025, 16, 10703−10711

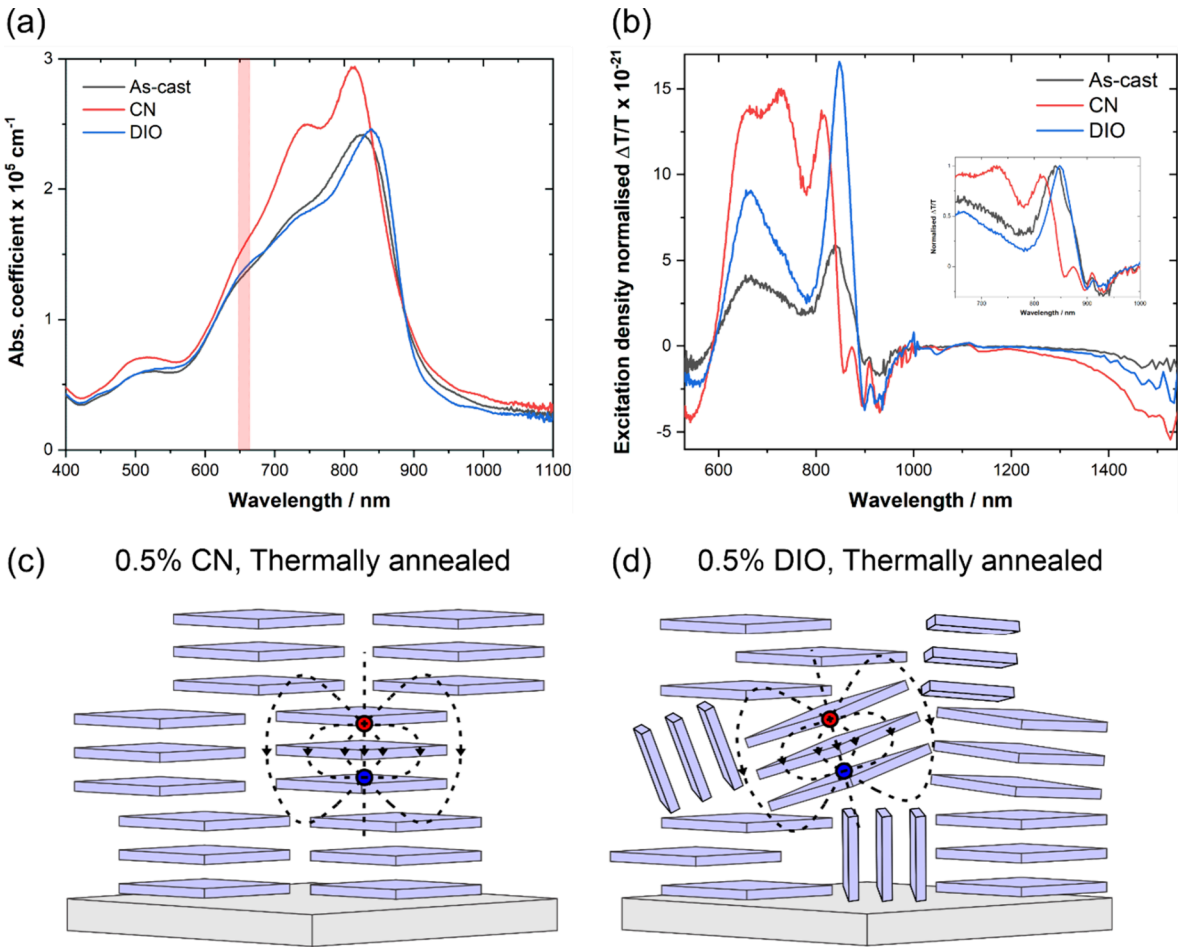

Figure 2. (a) Absorption coefficient of the thin films. The red rectangle highlights the pump bandwidth of 646−665 nm. (b) Excitation density normalized TA spectra for the thin films at 0.2−0.3 ps using 1.0 μJ cm^{-2} fluence. (c) CN-treated films have a greater long-range order as well as orientational order (face-on to the substrate). The electric field created by the separated electron hole pair in the intermolecular CT state impacts the absorption of the neighboring molecules which gives the TEA response. (d) DIO-treated films show more random orientational order (face-on and edge-on crystallites exist) and reduced long-range order.

we proposed that optimizing cofacial packing for device performance requires balancing cofacial dimer formation with the maintenance of face-on molecular orientation relative to the substrate—a structural configuration that solvent additives can help modulate.

Given the strong influence of solvent additives on Y6 morphology and the creation of intermolecular CT states, this material is ideal for exploring the impact of morphology on electronic interactions. In this study, we perform GIWAXS measurements and sub-55 fs transient absorption spectroscopy to structurally and dynamically characterize Y6 thin films. TEA spectra were extracted in the presence of different solvent additives to probe the nature of the formed intermolecular CT states. Consistent with previous literature,[5] our GIWAXS measurement of CN-treated Y6 film shows the presence of two out-of-plane peaks at 3.39 Å and 9.51 Å indicating greater long-range order than the as-cast or DIO-treated Y6 thin films. Spectral analysis of the extracted TEA reveals predominantly second-derivative character for CN-treated Y6 films, and primarily first derivative features in DIO-treated films, directly suggesting the more delocalized nature of excitations in films treated with CN compared to DIO. We attribute this to enhanced core−core interactions and reduced energetic disorder in CN-treated films, leading to increased delocalization of the CT states therein. Furthermore, CN treatment accelerates the rise time of the intermolecular CT state by an order of magnitude, from 2 ps in DIO-treated films to just 0.2 ps. Notably, this trend aligns closely with the relative charge generation times observed in PM6:Y6 bulk heterojunctions processed with the same additives, which are 5.6 ps for DIO treatment and 0.6 ps for CN treatment.[32] These findings demonstrate that direct optical investigations on pristine acceptor films can provide actionable insights into the functional impact of processing additives, offering a streamlined and predictive approach for additive design and OPV optimization.

Thin films of neat Y6 were prepared by incorporating 0.5 vol % of either CN or DIO as additives and thermally annealing at 80 °C for 10 min followed by encapsulation by a UV-curable glue (see SI section 2 for details). This procedure was adapted from established protocols for optimized PM6:Y6[9] and neat Y6 devices.[9,33] Detailed film fabrication procedures are described in the SI section 1. Figure 1a displays the molecular structures of Y6 and the additives and Figure 1b shows the normalized absorption and photoluminescence (PL) spectra of the thin films. The film prepared with CN exhibits a blue shift in the 0−0 absorption and a reduced 0−0 to 0−1 absorption peak ratio, suggesting a higher degree of cofacial H-like aggregation

https://doi.org/10.1021/acs.jpclett.5c02643
J. Phys. Chem. Lett. 2025, 16, 10703−10711

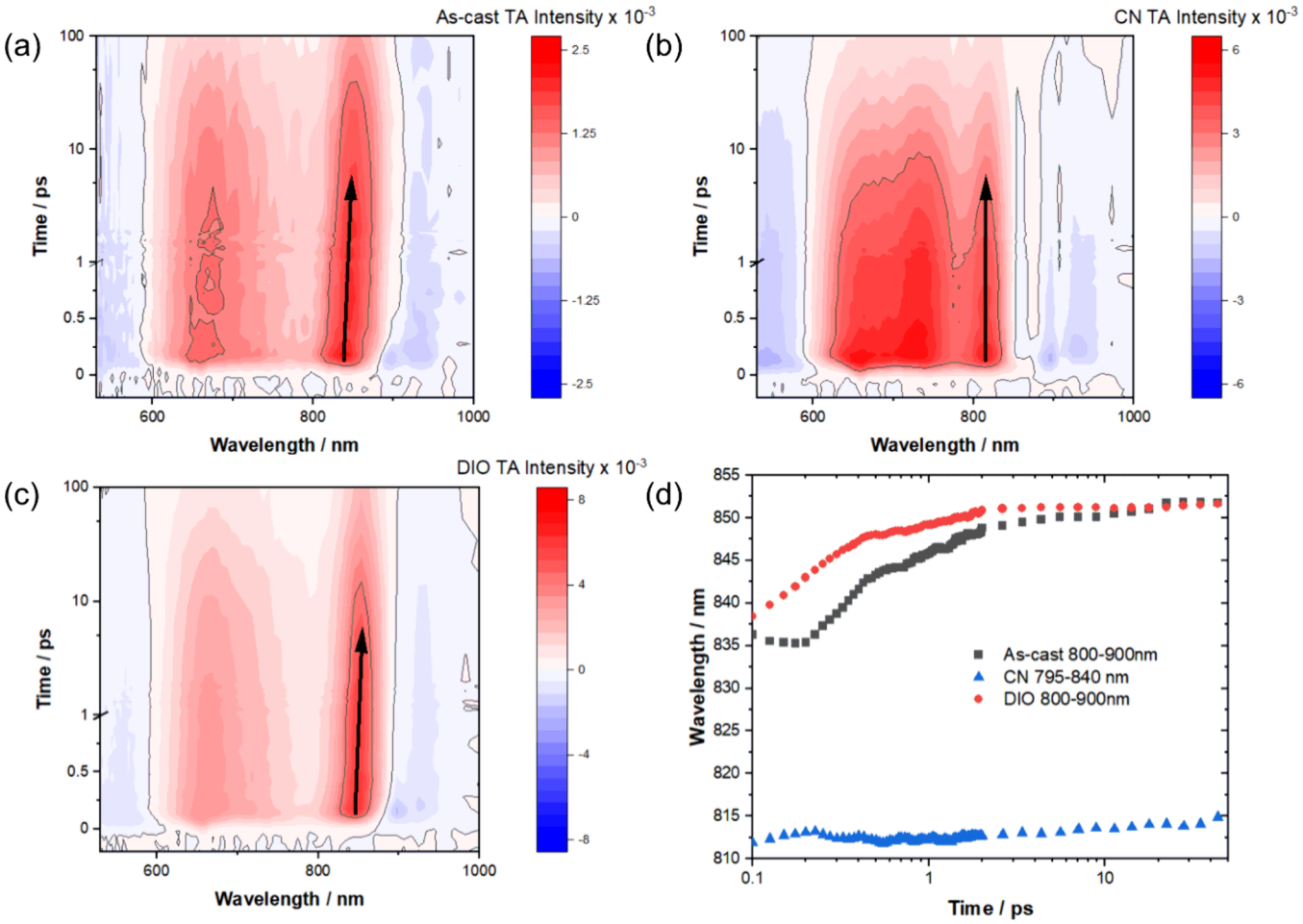

Figure 3. TA 2D spectrograms for (a) as-cast, (b) CN-treated, and (c) DIO-treated Y6 films. The arrows trace the evolution of the bleach. In the case of as-cast and DIO-treated films, a clear red shift of the bleach is observed, whereas this is minimal in the CN-treated film. (d) Peak wavelength shift for the three films as a function of time. The peaks were taken from the wavelength region mentioned in the legend.

among the Y6 molecules.[31,34] In contrast, the film with DIO shows a red-shifted absorption relative to the as-cast film and a slightly increased 0−0 to 0−1 peak ratio, indicating a preference for end-on aggregation in the thin film.[31,34] It is worth pointing out that Y6 forms multiple dimer conformations, which include tail−tail, core−core, tail−core, and core:core−tail:tail interactions (shown in SI section 3).[9,35] Given this complexity, dimers in the thin films cannot be described as being strictly H- or J-aggregates. Rather, as before,[31] we use the absorption peak ratios to infer different extents of cofacial interactions in thin films prepared with no additive, 0.5% CN, and 0.5% DIO. Importantly both CN (161 meV) and DIO (154 meV) show a reduced Stokes shift compared to the as-cast film (196 meV) (see SI section 4 for details) suggesting that the films with additives have more rigid molecular packing with reduced disorder. Increased rigidity in the films treated with additives can also be inferred from the blue shift of their PL peak compared to the as-cast film.[28] Spectrally, the shape of DIO-treated film's PL is similar to that of the as-cast, while the CN-treated film depicts a sharp onset of the PL as well as pronounced spectral narrowing. Interestingly, such a PL shape was previously observed in highly crystalline domains in microscopic PL measurements[31] suggesting a high degree of crystallinity in thin films prepared with CN additive. Moreover, the photoluminescence quantum yield of the CN-treated film was found to be the highest among all at 8% compared to 6 and 4% for the as-cast and DIO-treated films respectively (SI section 4).

GIWAXS reveals clear differences in molecular orientation and structural ordering among the Y6 thin films (Figure 1c−e). Both CN- and DIO-treated films exhibit a reduced $\pi-\pi$ stacking distance, with the (010) out-of-plane peak corresponding to ∼3.39 Å, compared to 3.41 Å for the as-cast film, indicating tighter vertical packing. Notably, the CN-treated film shows an additional out-of-plane peak at $q_z \approx 0.66$ Å^{-1} ($d \approx 9.51$ Å), consistent with previous reports by Zhang et al.[5] and corresponds to lamellar stacking of CN-treated Y6 films. This suggests improved long-range ordering in the vertical direction. The out-of-plane peaks of the CN-treated film are also sharper and more intense, pointing to a predominantly face-on molecular orientation. Furthermore, the CN-treated film displays the shortest in-plane spacing, ∼19 Å, compared with 22 Å for the as-cast film and 24 Å for the DIO-treated film, suggesting tighter molecular packing along the in-plane direction. In contrast, the GIWAXS pattern (SI section 5) of the DIO-treated film presents a complete diffraction ring for the (010) peak, indicating randomly oriented crystallites.

Femtosecond TA measurements with <55 fs time resolution, using a 655 nm pump and variable fluences (1.0, 3.0, 9.1, and 12.1 μJ cm^{-2}) were performed to investigate the photophysics of the fabricated Y6 thin films. The absorption coefficient of the as-cast film is quite similar to that of the additive treated

https://doi.org/10.1021/acs.jpclett.5c02643
J. Phys. Chem. Lett. 2025, 16, 10703−10711

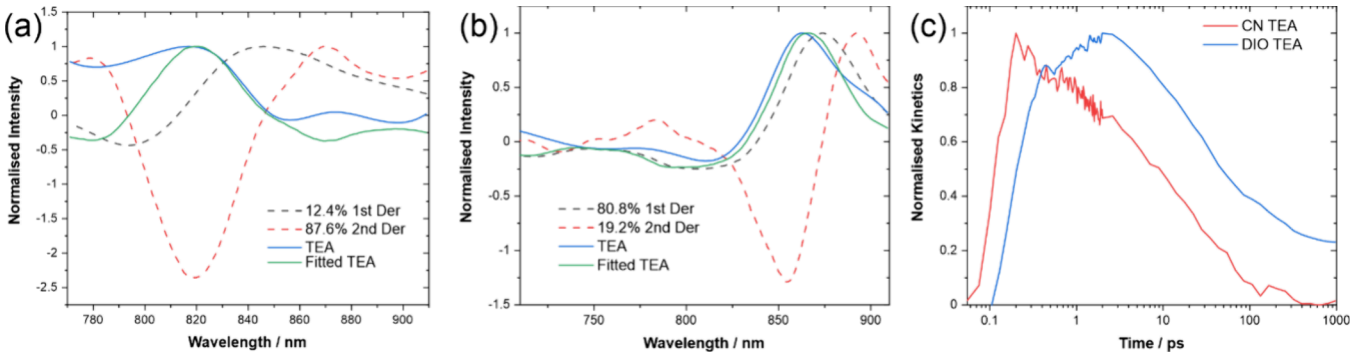

Figure 4. (a, b) Fits of the extracted TEA using the first and second derivatives of the absorption spectra for (a) CN-treated and (b) DIO-treated films. TEA is extracted by performing genetic algorithm (GA) on the 1 μJ cm^{-2} TA data after taking a reference spectral mask at 50 fs in both cases. The legend indicates the contribution of each derivative toward the fitting. (c) Rise of the TEA signal that was extracted by GA.

films (Figure 2a). However, when the TA signal is normalized by the excitation density, we observe a strong enhancement of the positive ground state bleach and the negative photo-induced absorption signals in films treated with both CN and DIO additives (Figure 2b) at early times. This suggests that additive treatment influences molecular aggregation in the thin films such that pairs of molecules are bleached, increasing the apparent population of excited states and thereby enhancing the TA signal. Enhancements in TA signal have been previously reported in PM6:Y-series acceptor BHJ thin films when CN and DIO were introduced, and was attributed to favorable phase separation in the BHJ upon additive treatment and reduced donor/acceptor CT state recombination on the nanosecond time scale.[14] While this may explain signal enhancements on the nanosecond time scale, reduced intermolecular CT state recombination is unlikely to explain the signal increase observed here on the subpicosecond time scale. We therefore propose that the increased number of sites for intermolecular CT state generation post additive treatment underlies this enhancement in the TA signal. This aligns with previous MD simulations, which showed that both additives increase the population of 'other' dimer pairs, where core:core-tail:tail interactions are most prevalent.[9] A higher population of these pairs could facilitate intermolecular CT state generation, as we and others have previously observed.[31,36]

Although both additives enhance the signal, the distinct shapes of their bleach features suggest that different predominant species contribute to the intermolecular CT states in the two films. The strong 0−0 bleach in DIO-treated films indicates that intermolecular CT states are primarily populated in more slip-stacked configurations. In contrast, the strong 0−1 bleach observed with CN suggests that intermolecular CTs are generated at sites with greater core−core overlap. These spectral features not only correspond with the steady-state absorption differences mentioned earlier but also align with all-atom MD simulations which predicted that the linear additive DIO reduces the number of core−core dimer pairs.[9] TA spectra of all studied films show a positive−negative derivative-like signal at the band edge around 900 nm which is characteristic of EA (inset of Figure 2b). Importantly, the ground state bleach of the CN-treated film exhibits an additional and distinct EA response characterized by a pronounced and sharp suppression of the signal between 850−870 nm (inset of Figure 2b). This feature is notably absent in both the as-cast and DIO-treated films. If this effect were solely due to a blue shift, the entire TA spectrum would have shifted accordingly. However, since the 660 nm bleach remains fixed at 660 nm across all films, it is evident that the CN-treated film exhibits a stronger EA contribution, leading to a more pronounced reduction in its band-edge bleach compared to the other two films. This enhanced EA response in the CN film is consistent with its greater film ordering, which likely amplify the absorption changes of neighboring molecules (see Figure 2c). In contrast, the EA signal in the DIO-treated film may be suppressed due to increased molecular disorder, which disrupts the cooperative electronic interactions within the film (see Figure 2d). Additionally, comparing the excitation density normalized photoinduced absorption at 1500 nm (Figure 2b) also suggests that the CN-treated film has more intermolecular CT states,[2] which is consistent with a stronger EA signal.

Previous work[23] found that following above band gap excitation, temporal red shift of the ground state bleach is universal in thin films of Y-series acceptors and is linked to the migration of the LE in amorphous regions of the film to more ordered low energy regions which contain tightly packed aggregates with sites conducive for intermolecular CT state generation. Interestingly, for the samples we studied and excited with above-band gap energy, as-cast and DIO-treated films show considerable and similar red shifts, while the bleach of the CN-treated film red-shifts only slightly (see Figure 3d). This highlights the high degree of energetic order and the presence of few amorphous regions in this film, which means that the initial excitation likely already exists in tightly packed sites. Additionally, normalized sub-0.2 ps spectral slices (SI section 6) reveal pronounced spectral broadening of the bleach in the as-cast film, which is absent in additive-treated samples − further indicating higher disorder in the as-cast film, potentially due to the lack of thermal annealing.

Although EA-related features have now been identified in the TA data, qualitatively indicating a stronger EA effect in the CN-processed film, spectral decomposition is required to isolate the 'pure' TEA contribution. Numerical approaches based on genetic algorithms (GA) are commonly employed to decompose overlapping signals in TA spectrograms, enabling the extraction of clean spectra and kinetics.[3,23,37−41] In a previous study,[23] the 0.2 ps spectrum was used as a reference mask for the LE to facilitate the extraction of the TEA spectrum and kinetics via GA. However, in the case of the CN-treated film, we find that 0.2 ps is too late, as the EA signature has already fully emerged in the spectrum. The raw spectral evolution at the subpicosecond time scale is provided in SI

https://doi.org/10.1021/acs.jpclett.5c02643
J. Phys. Chem. Lett. 2025, 16, 10703−10711

section 6. Moreover, since we did not observe a pronounced red shift of the ground state bleach in the case of the CN-treated film, it is likely that the initially populated state already shows significant intermolecular CT character. Hence, we used the earliest time slice of ∼50 fs (for each film) as a reference or mask for GA to extract the TEA shape and its kinetics (SI section 7). The extracted TEA spectra from the lowest fluence measurement were then fit using the first and second derivatives of the absorption spectrum (on an energy scale, but plotted in Figure 4 on the wavelength scale).

Interestingly, we find that CN-treated film shows almost 90% second derivative character of the TEA spectrum while DIO-treated film shows around 80% first derivative character (Figure 4a,b). This highlights a clear difference between the nature of the intermolecular CT states in the two films. Moreover, we find that the TEA signal in CN-treated film rises 10 times faster than the DIO-treated film (0.2 and 2 ps, respectively; Figure 4c). Our results indicate that CN-induced H-type interactions stabilize intermolecular CT states, leading to enhanced CT hybridization and/or greater charge separation. Both effects are expected to increase the CT character of the S_1 state and thereby yield a stronger second-derivative EA response. Moreover, DFT calculations based on MD simulations have shown that CN treatment increases the Y6 intermolecular binding energy (0.10 → 2.20 eV),[42] consistent with stronger $\pi-\pi$ interactions. Accordingly, the CN-treated film exhibits a more intense EA signal than the DIO-treated counterpart, which we attribute to its higher degree of molecular order and the larger population of CT states.

The TEA rise time in our as-cast film (∼2 ps) closely aligns with the previously reported value of 2.9 ps (see SI section 8 for a discussion on TEA fits for the as-cast film). Notably, since the addition of CN shortens the TEA rise time by an order of magnitude, this proves solvent additive engineering to be an effective and straightforward strategy for modulating photophysics without necessitating the synthesis of new materials. While previous studies have suggested that reduced intermolecular interactions accelerate TEA rise times, as exemplified by the sterically hindered Y-type molecule L8-BO, which exhibits the fastest reported TEA dynamics at 1 ps,[23] our findings challenge this notion. In the presence of CN, we observe stronger core−core intermolecular interactions (i.e., H-type character, as supported by the shape of the steady-state absorption spectrum and the ground-state bleach in TA), enhanced in-plane packing density (which is expected to increase the $\pi-\pi$ contact area between molecules), and yet an exceptionally fast TEA rise time of 0.2 ps, surpassing even the L8-BO case. It is important to distinguish the LE to intermolecular CT transfer time probed via TEA from the subpicosecond LE to intermolecular CT conversion observed in Y6.[2,31] As the intermolecular CT state is generated on the subpicosecond time scale in the film, it alters the absorption of the neighboring molecules. This process will have a delayed response time compared to the generation of the intermolecular CT state itself. Of the studied samples, the CN-treated film shows the least fluence dependence of the photoinduced absorption signal of the LE decay (SI section 9). This further confirms that the nanomorphology of the CN-treated film allows for the least diffusion limited intermolecular CT state generation matching the fastest TEA rise observed in this film.

Comparing the spectral fitting errors for CN and DIO-treated films in Figure 4, it is evident that while the TEA spectrum of the DIO-treated film is well described by the derivatives of the absorption spectrum, the fit for the CN-treated film is less accurate (residual sum of squares is given in SI section 7). Similar challenges in fitting EA spectra using first and second derivatives have been observed in thermally activated delayed fluorescence molecules, where strong mixing between the triplet and CT states was reported.[43] Notably, this mixing enhanced the thermally activated delayed fluorescence performance compared to molecules lacking such state interaction. In our case, we speculate that the enhanced core−core interactions lead to greater intermolecular CT state stabilization, resulting in stronger mixing between the LE and intermolecular CT states. This enhanced mixing could explain the poorer agreement between the CN-treated film's TEA spectrum and derivative-based fits compared to DIO.

While this study focuses on neat Y6 films, it is informative to consider how the choice of additive influences the V_{oc} in full BHJ devices comprising PM6:Y6. Several reports[9,15,32,42] (see Figure S12) have investigated the impact of CN and DIO on PM6:Y6 OPVs and, despite variations in fabrication conditions, a consistent trend emerges: DIO treatment results in the lowest V_{oc}. This persistent degradation in V_{oc} upon DIO treatment may reflect increased energetic and structural disorder and higher defect densities, as also suggested by reduced PLQE and broader absorption features in DIO-treated films. Although morphological and processing differences limit direct comparisons across studies, the consistent observation of lower V_{oc} with DIO supports our interpretation that additive-induced changes to intermolecular interactions—and their consequences on electronic structure—are central to OPV performance.

This interpretation is further supported by studies beyond PM6:Y6. In the case of BTIC-CF3-m,[44] a Y-type acceptor, DIO treatment caused a marked reduction in V_{oc} attributed to enhanced end-on or J-type aggregation, which reduces the effective bandgap. By contrast, CN maintained the V_{oc} of the pristine blend. Moreover, a recent comprehensive study[32] evaluating all combinations of two high-performing polymer donors (PM6 and D18-Fu) with two benchmark acceptors (Y6 and L8-BO) found that, across all 12 device configurations, CN consistently resulted in lower V_{oc} loss compared to DIO. These broader trends reinforce the idea that conjugated additives like CN are generally better suited than aliphatic ones like DIO for preserving favorable electronic properties in Y-type acceptor-based OPVs.

Both CN and DIO treatments have been reported to enhance the short-circuit current density (J_{sc}) in PM6:Y6 devices, as shown in Figure S12b. For DIO-treated blends, this enhancement has been attributed to a red shift in the absorption spectrum, which improves light harvesting by extending spectral coverage. In contrast, the increase in J_{sc} observed for CN-treated blends is less intuitive, as their absorption spectra appear nearly identical to those of pristine films.[9] We note that the spectra presented in the reference are normalized, and therefore do not allow for direct comparison of absorption coefficients. Despite this limitation, we propose that the observed enhancement in J_{sc} with CN treatment may stem from improved intrinsic charge photogeneration − potentially facilitated by enhanced intermolecular coupling and reduced energetic disorder. This hypothesis is supported by the reduced fluence dependence of the LE photoinduced absorption decay observed in CN-treated neat films (SI section 7). While we acknowledge that extrapolating from neat film

https://doi.org/10.1021/acs.jpclett.5c02643
J. Phys. Chem. Lett. 2025, 16, 10703−10711

dynamics to blend device performance has inherent limitations, these results suggest that CN incorporation may promote more efficient charge generation and extraction, consistent with the reported device-level improvements.

Our findings demonstrate that the inherent ability of Y-series acceptors to form intermolecular CT states and generate internal fields can be leveraged to probe the distinct microenvironments in thin films stemming from differences in nanomorphology. This approach is particularly relevant given that modern non-fullerene acceptors largely retain their crystalline packing within BHJ active layers[5,23,45−48] and that, in contemporary OPVs, energy transfer from the donor to the acceptor occurs rapidly, making the acceptor the primary precursor for charge generation.[49] Furthermore, our study underscores the crucial role of additive engineering in tuning intermolecular CT state characteristics through morphology modulation, offering a complementary strategy compared to the design and synthesis of novel acceptors. Specifically, the conjugated additive CN enhances long-range molecular order and increases the in-plane molecular packing density (as indicated by our GIWAXS data), leads to a smaller red shift in the ground-state bleach, and promotes greater core−core dimer formation (as reflected in the relative intensities of the 0−0 and 0−1 absorption peaks). This structural arrangement facilitates the ultrafast generation of intermolecular CT states with a strong second derivative character, indicative of greater electron−hole separation and delocalization. As mentioned earlier, the findings of our previous work,[31] suggested that optimizing cofacial packing for device performance requires balancing cofacial dimer formation while maintaining a face-on molecular orientation relative to the substrate. The results of this study suggest that the CN-treated film achieves this favorable structural configuration, which may explain its superior performance compared to DIO-treated BHJ devices. The ability to directly evaluate the functional effectiveness of additives in thin films via direct optical probes offers a valuable approach for future additive development, aiding in the design and selection of new additives.

■ ASSOCIATED CONTENT

Supporting Information

The Supporting Information is available free of charge at https://pubs.acs.org/doi/10.1021/acs.jpclett.5c02643.

Information regarding experimental methods, thin-film UV-encapsulation effects, absolute photoluminescence quantum yield, 2D GWIAXS patterns, subpicosecond raw spectral evolution, transient electroabsorption fitting and a discussion on as-cast transient electroabsorption, fluence dependence of photoinduced absorption dynamics, and PM6:Y6 device performance (PDF)

■ AUTHOR INFORMATION

Corresponding Authors

Bo-Han Chen − *Institute of Photonics Technologies, National Tsing Hua University, Hsinchu 300044, Taiwan*; Email: bohan.chen@ee.nthu.edu.tw

Paul A. Hume − *School of Chemical and Physical Sciences, Victoria University of Wellington, Wellington 6012, New Zealand; MacDiarmid Institute for Advanced Materials and Nanotechnology, Wellington 6012, New Zealand*; orcid.org/0000-0002-7582-7155; Email: paul.hume@vuw.ac.nz

Justin M. Hodgkiss − *School of Chemical and Physical Sciences, Victoria University of Wellington, Wellington 6012, New Zealand; MacDiarmid Institute for Advanced Materials and Nanotechnology, Wellington 6012, New Zealand*; orcid.org/0000-0002-9629-8213; Email: justin.hodgkiss@vuw.ac.nz

Kai Chen − *MacDiarmid Institute for Advanced Materials and Nanotechnology, Wellington 6012, New Zealand; The Dodd-Walls Centre for Photonic and Quantum Technologies, Dunedin 9016, New Zealand; Robinson Research Institute, Faculty of Engineering, Victoria University of Wellington, Wellington 6012, New Zealand*; orcid.org/0000-0002-3591-4238; Email: kai.chen@vuw.ac.nz

Authors

Aditi Kumar − *School of Chemical and Physical Sciences, Victoria University of Wellington, Wellington 6012, New Zealand; MacDiarmid Institute for Advanced Materials and Nanotechnology, Wellington 6012, New Zealand; The Dodd-Walls Centre for Photonic and Quantum Technologies, Dunedin 9016, New Zealand*; orcid.org/0009-0008-0555-1086

Chao-Yang Lin − *MacDiarmid Institute for Advanced Materials and Nanotechnology, Wellington 6012, New Zealand; The Dodd-Walls Centre for Photonic and Quantum Technologies, Dunedin 9016, New Zealand; Robinson Research Institute, Faculty of Engineering, Victoria University of Wellington, Wellington 6012, New Zealand*

Nikita A. Shumilov − *School of Chemical and Physical Sciences, Victoria University of Wellington, Wellington 6012, New Zealand; MacDiarmid Institute for Advanced Materials and Nanotechnology, Wellington 6012, New Zealand; The Dodd-Walls Centre for Photonic and Quantum Technologies, Dunedin 9016, New Zealand*; orcid.org/0000-0002-6694-9118

Nathaniel J. L. K. Davis − *School of Chemical and Physical Sciences, Victoria University of Wellington, Wellington 6012, New Zealand; MacDiarmid Institute for Advanced Materials and Nanotechnology, Wellington 6012, New Zealand; The Dodd-Walls Centre for Photonic and Quantum Technologies, Dunedin 9016, New Zealand*; orcid.org/0000-0003-2535-8968

Yu-Chiang Chao − *Department of Physics, National Taiwan Normal University, Taipei 11677, Taiwan*; orcid.org/0000-0002-9831-9292

Li-Kang Chu − *Department of Chemistry, National Tsing Hua University, Hsinchu 30013, Taiwan*; orcid.org/0000-0001-6080-9598

Chia-Feng Li − *Department of Materials Science and Engineering, National Taiwan University, Taipei 10617, Taiwan*

Yu-Ching Huang − *Department of Materials Engineering and Organic Electronics Research Center, Ming Chi University of Technology, New Taipei City 24301, Taiwan*; orcid.org/0000-0003-4772-8050

Shang-Da Yang − *Institute of Photonics Technologies and College of Semiconductor Research, National Tsing Hua University, Hsinchu 300044, Taiwan*; orcid.org/0000-0003-3151-0700

Michael B. Price − *School of Chemistry, University of Bristol, Bristol BS8 1TS, United Kingdom*

Complete contact information is available at: https://pubs.acs.org/10.1021/acs.jpclett.5c02643

Author Contributions

A.K. prepared the samples, led the data analysis, visualization, and drafting of the manuscript and contributed equally to experimental investigations. B.-H.C. shared equal responsibility in experimental investigations. C.-Y.L. and N.A.S. provided supporting contributions to experiments. C.-F.L. and Y.-C.H. performed GIWAXS measurements and analysis. N.J.L.K.D., Y.-C.C., S.-D.Y., and L.-K.C. supported the project through resource provision. M.B.P. contributed to supervision and manuscript editing. P.A.H. shared supervisory responsibilities and contributed equally to manuscript review and editing. J.M.H. contributed equally to project supervision, funding acquisition, and manuscript revision. K.C. conceived the project, acquired funding, and contributed equally to supervision.

Notes

The authors declare no competing financial interest.

■ ACKNOWLEDGMENTS

A.K., K.C., P.A.H., and J.M.H. acknowledge support from the Marsden Fund of New Zealand. A.K. acknowledges the Te Whai Ao—Dodd-Walls Centre for the Ph.D. Output Award. M.B.P. acknowledges the support of the Royal Society (U.K.) for funding. N.J.L.K.D. acknowledges funding from the Royal Society of New Zealand - Te Aparangi. The authors would like to thank Dr. Chun-Yu Chen (TPS25A1) at the National Synchrotron Radiation Research Centre for helpful discussions.

■ REFERENCES

(1) Yuan, J.; Zhang, Y.; Zhou, L.; Zhang, G.; Yip, H. L.; Lau, T. K.; Lu, X.; Zhu, C.; Peng, H.; Johnson, P. A.; Leclerc, M.; Cao, Y.; Ulanski, J.; Li, Y.; Zou, Y. Single-Junction Organic Solar Cell with over 15% Efficiency Using Fused-Ring Acceptor with Electron-Deficient Core. *Joule* **2019**, *3* (4), 1140−1151.

(2) Wang, R.; Zhang, C.; Li, Q.; Zhang, Z.; Wang, X.; Xiao, M. Charge Separation from an Intra-Moiety Intermediate State in the High-Performance PM6:Y6 Organic Photovoltaic Blend. *J. Am. Chem. Soc.* **2020**, *142* (29), 12751−12759.

(3) Price, M. B.; Hume, P. A.; Ilina, A.; Wagner, I.; Tamming, R. R.; Thorn, K. E.; Jiao, W.; Goldingay, A.; Conaghan, P. J.; Lakhwani, G.; Davis, N. J. L. K.; Wang, Y.; Xue, P.; Lu, H.; Chen, K.; Zhan, X.; Hodgkiss, J. M. Free Charge Photogeneration in a Single Component High Photovoltaic Efficiency Organic Semiconductor. *Nat. Commun.* **2022**, *13*, No. 2827.

(4) Zhu, L.; Zhang, J.; Guo, Y.; Yang, C.; Yi, Y.; Wei, Z. Small Exciton Binding Energies Enabling Direct Charge Photogeneration Towards Low-Driving-Force Organic Solar Cells. *Angew. Chem., Int. Ed.* **2021**, *60* (28), 15348−15353.

(5) Zhang, G.; Chen, X. K.; Xiao, J.; Chow, P. C. Y.; Ren, M.; Kupgan, G.; Jiao, X.; Chan, C. C. S.; Du, X.; Xia, R.; Chen, Z.; Yuan, J.; Zhang, Y.; Zhang, S.; Liu, Y.; Zou, Y.; Yan, H.; Wong, K. S.; Coropceanu, V.; Li, N.; Brabec, C. J.; Bredas, J. L.; Yip, H. L.; Cao, Y. Delocalization of Exciton and Electron Wavefunction in Non-Fullerene Acceptor Molecules Enables Efficient Organic Solar Cells. *Nat. Commun.* **2020**, *11*, No. 3943.

(6) Zhu, L.; Zhang, M.; Xu, J.; Li, C.; Yan, J.; Zhou, G.; Zhong, W.; Hao, T.; Song, J.; Xue, X.; Zhou, Z.; Zeng, R.; Zhu, H.; Chen, C. C.; MacKenzie, R. C. I.; Zou, Y.; Nelson, J.; Zhang, Y.; Sun, Y.; Liu, F. Single-Junction Organic Solar Cells with over 19% Efficiency Enabled by a Refined Double-Fibril Network Morphology. *Nat. Mater.* **2022**, *21* (6), 656−663.

(7) Meng, L.; Liang, H.; Song, G.; Li, M.; Huang, Y.; Jiang, C.; Zhang, K.; Huang, F.; Yao, Z.; Li, C.; Wan, X.; Chen, Y. Tandem Organic Solar Cells with Efficiency over 19% via the Careful Subcell Design and Optimization. *Sci. China: Chem.* **2023**, *66* (3), 808−815.

(8) Moustafa, E.; Torimtubun, A. A. A.; Pallarès, J.; Marsal, L. F. Effect of Additives and Annealing on the Performance of Non-fullerene-Based Binary and Ternary Organic Photovoltaics. *Solar RRL* **2022**, *6* (5), No. 2100480.

(9) Xia, X.; Mei, L.; He, C.; Chen, Z.; Yao, N.; Qin, M.; Sun, R.; Zhang, Z.; Pan, Y.; Xiao, Y.; Lin, Y.; Min, J.; Zhang, F.; Zhu, H.; Bredas, J. L.; Chen, H.; Chen, X. K.; Lu, X. Revealing the Crystalline Packing Structure of Y6 in the Active Layer of Organic Solar Cells: The Critical Role of Solvent Additives. *J. Mater. Chem. A* **2023**, *11* (40), 21895−21907.

(10) Zhu, L.; Zhang, M.; Zhou, G.; Hao, T.; Xu, J.; Wang, J.; Qiu, C.; Prine, N.; Ali, J.; Feng, W.; Gu, X.; Ma, Z.; Tang, Z.; Zhu, H.; Ying, L.; Zhang, Y.; Liu, F. Efficient Organic Solar Cell with 16.88% Efficiency Enabled by Refined Acceptor Crystallization and Morphology with Improved Charge Transfer and Transport Properties. *Adv. Energy Mater.* **2020**, *10* (18), No. 1904234.

(11) Lv, J.; Tang, H.; Huang, J.; Yan, C.; Liu, K.; Yang, Q.; Hu, D.; Singh, R.; Lee, J.; Lu, S.; Li, G.; Kan, Z. Additive-Induced Miscibility Regulation and Hierarchical Morphology Enable 17.5% Binary Organic Solar Cells. Energy. *Environ. Sci.* **2021**, *14* (5), 3044−3052.

(12) Shoaee, S.; Luong, H. M.; Song, J.; Zou, Y.; Nguyen, T. Q.; Neher, D. What We Have Learnt from PM6:Y6. *Adv. Mater.* **2024**, *36*, No. 2302005.

(13) Raab, T.; Seewald, T.; Kraner, S.; Schmidt-Mende, L. Uncovering Solvent-Engineering Mechanisms in Y6:PM6 Solar Cells. *APL Mater.* **2023**, *11*, No. 051116.

(14) Ham, G.; Lee, D.; Park, C.; Cha, H. Charge Carrier Dynamics in Non-Fullerene Acceptor-Based Organic Solar Cells: Investigating the Influence of Processing Additives Using Transient Absorption Spectroscopy. *Materials* **2023**, *16*, No. 5712.

(15) Shen, Z.; Yu, J.; Lu, G.; Wu, K.; Wang, Q.; Bu, L.; Liu, X.; Zhu, Y.; Lu, G. Surface Crystallinity Enhancement in Organic Solar Cells Induced by Spinodal Demixing of Acceptors and Additives. *Energy Environ. Sci.* **2023**, *16* (7), 2945−2956.

(16) Mei, L.; Xia, X.; Sun, R.; Pan, Y.; Min, J.; Lu, X.; Jen, A. K. Y.; Chen, X. K. Molecular-Level Insight into Impact of Additives on Film Formation and Molecular Packing in Y6-Based Organic Solar Cells. *Small* **2024**, *20*, No. 2305977.

(17) Ziffer, M. E.; Mohammed, J. C.; Ginger, D. S. Electroabsorption Spectroscopy Measurements of the Exciton Binding Energy, Electron-Hole Reduced Effective Mass, and Band Gap in the Perovskite $CH_3NH_3PbI_3$. *ACS Photonics* **2016**, *3* (6), 1060−1068.

(18) Jalviste, E.; Ohta, N. Theoretical Foundation of Electroabsorption Spectroscopy: Self-Contained Derivation of the Basic Equations with the Direction Cosine Method and the Euler Angle Method. *J. Photochem. Photobiol., C* **2007**, *8* (1), 30−46.

(19) Liu, T.; Foo, Y.; Zapien, J. A.; Li, M.; Tsang, S. W. A Generalized Stark Effect Electromodulation Model for Extracting Excitonic Properties in Organic Semiconductors. *Nat. Commun.* **2019**, *10*, No. 5089.

(20) Gulbinas, V.; Kananavičius, R.; Valkunas, L.; Bässler, H. Dynamic Stark Effect as a Probe of the Evolution of Geminate Electron-Hole Pairs in a Conjugated Polymer. *Phys. Rev. B: Condens. Matter Mater. Phys.* **2002**, *66* (23), No. 233203.

(21) Bublitz, G. U.; Boxer, S. G. Stark Spectroscopy: Applications in Chemistry, Biology, and Materials Science. *Annu. Rev. Phys. Chem.* **1997**, *48* (1), 213−242.

(22) Scarongella, M.; De Jonghe-Risse, J.; Buchaca-Domingo, E.; Causa', M.; Fei, Z.; Heeney, M.; Moser, J. E.; Stingelin, N.; Banerji, N. A Close Look at Charge Generation in Polymer: Fullerene Blends with Microstructure Control. *J. Am. Chem. Soc.* **2015**, *137* (8), 2908−2918.

(23) Guo, Y.; Han, G.; Guo, J.; Guo, H.; Fu, Y.; Miao, X.; Wang, Z.; Li, D.; Li, S.; Xu, X.; Lu, X.; Chen, H.; Yi, Y.; Chow, P. C. Y. Engineering Ultrafast Exciton Dynamics to Boost Organic Photovoltaic Performance. *Energy Environ. Sci.* **2024**, *17* (22), 8776−8786.

(24) Mahadevan, S.; Liu, T.; Pratik, S. M.; Li, Y.; Ho, H. Y.; Ouyang, S.; Lu, X.; Yip, H.-L.; Chow, P. C. Y.; Brédas, J.-L.; Coropceanu, V.; So, S. K.; Tsang, S.-W. Assessing Intra- and Inter-Molecular Charge

https://doi.org/10.1021/acs.jpclett.5c02643
J. Phys. Chem. Lett. 2025, 16, 10703−10711

Transfer Excitations in Non-Fullerene Acceptors Using Electroabsorption Spectroscopy. *Nat. Commun.* **2024**, *15*, No. 2393.
(25) Li, M.; Qin, Y.; Dai, W.; Luo, X. Tuning the Performance of the Non-Fullerene Organic Solar Cells by the Polarizability. *RSC Adv.* **2018**, *8* (7), 3809−3815.
(26) Martin, S. J.; Mellor, H.; Bradley, D. D. C.; Burn, P. L. Electroabsorption Studies of PPV and MEH-PPV. *Opt Mater.* **1998**, *9* (1−4), 88−93.
(27) Bothra, U.; Westbrook, R. J. E.; Liu, Y.; Wang, J.; Ziffer, M. E.; Ginger, D. S. Probing Charge Transfer Character in Modern Donor/Acceptor Materials via Electroabsorption Spectroscopy. *J. Phys. Chem. Lett.* **2024**, *15* (5), 1288−1293.
(28) Legaspi, C. M.; Stubbs, R. E.; Wahadoszaman, M.; Yaron, D. J.; Peteanu, L. A.; Kemboi, A.; Fossum, E.; Lu, Y.; Zheng, Q.; Rothberg, L. J. Rigidity and Polarity Effects on the Electronic Properties of Two Deep Blue Delayed Fluorescence Emitters. *J. Phys. Chem. C* **2018**, *122* (22), 11961−11972.
(29) Bernardo, B.; Cheyns, D.; Verreet, B.; Schaller, R. D.; Rand, B. P.; Giebink, N. C. Delocalization and Dielectric Screening of Charge Transfer States in Organic Photovoltaic Cells. *Nat. Commun.* **2014**, *5*, No. 3245.
(30) Lin, Y.; Wang, J.; Zhang, Z. G.; Bai, H.; Li, Y.; Zhu, D.; Zhan, X. An Electron Acceptor Challenging Fullerenes for Efficient Polymer Solar Cells. *Adv. Mater.* **2015**, *27* (7), 1170−1174.
(31) Kumar, A.; Hudson, R. J.; Shumilov, N. A.; Lin, C.; Smith, T. A.; Davis, N. J. L. K.; Le Ru, E. C.; Price, M. B.; Hume, P. A.; Hodgkiss, J. M. Morphological Control of Y6 Thin Films Reveals Charge Transfer Is Facilitated by Co-Facial Interactions. *J. Phys. Chem. Lett.* **2025**, *16*, 1367−1375.
(32) Chen, L.; Ma, R.; Yi, J.; Dela Peña, T. A.; Li, H.; Wei, Q.; Yan, C.; Wu, J.; Li, M.; Cheng, P.; Yan, H.; Zhang, G.; Li, G. Exploiting the Donor-Acceptor-Additive Interaction's Morphological Effect on the Performance of Organic Solar Cells. *Aggregate* **2024**, *5*, No. e4455.
(33) Sağlamkaya, E.; Musiienko, A.; Shadabroo, M. S.; Sun, B.; Chandrabose, S.; Shargaieva, O.; Lo Gerfo, M. G.; van Hulst, N. F.; Shoaee, S. What Is Special about Y6; the Working Mechanism of Neat Y6 Organic Solar Cells. *Mater. Horiz* **2023**, *10*, 1825−1834.
(34) Spano, F. C. The Spectral Signatures of Frenkel Polarons in H- and J-Aggregates. *Acc. Chem. Res.* **2010**, *43* (3), 429−439.
(35) Kroh, D.; Eller, F.; Schötz, K.; Wedler, S.; Perdigón-Toro, L.; Freychet, G.; Wei, Q.; Dörr, M.; Jones, D.; Zou, Y.; Herzig, E. M.; Neher, D.; Köhler, A. Identifying the Signatures of Intermolecular Interactions in Blends of PM6 with Y6 and N4 Using Absorption Spectroscopy. *Adv. Funct Mater.* **2022**, *32*, No. 2205711.
(36) Yuk, D.; Jee, M. H.; Koh, C. W.; Park, W.-W.; Ryu, H. S.; Lee, D.; Cho, S.; Rasool, S.; Park, S.; Kwon, O.-H.; Kim, J. Y.; Woo, H. Y. Simplified Y6-Based Nonfullerene Acceptors: In-Depth Study on Molecular Structure-Property Relation, Molecular Dynamics Simulation, and Charge Dynamics. *Small* **2023**, *19*, No. 2206547.
(37) Schwarz, K. N.; Geraghty, P. B.; Mitchell, V. D.; Khan, S. U. Z.; Sandberg, O. J.; Zarrabi, N.; Kudisch, B.; Subbiah, J.; Smith, T. A.; Rand, B. P.; Armin, A.; Scholes, G. D.; Jones, D. J.; Ghiggino, K. P. Reduced Recombination and Capacitor-like Charge Buildup in an Organic Heterojunction. *J. Am. Chem. Soc.* **2020**, *142* (5), 2562−2571.
(38) Chow, P. C. Y.; Gélinas, S.; Rao, A.; Friend, R. H. Quantitative Bimolecular Recombination in Organic Photovoltaics through Triplet Exciton Formation. *J. Am. Chem. Soc.* **2014**, *136* (9), 3424−3429.
(39) Rao, A.; Chow, P. C. Y.; Gélinas, S.; Schlenker, C. W.; Li, C. Z.; Yip, H. L.; Jen, A. K. Y.; Ginger, D. S.; Friend, R. H. The Role of Spin in the Kinetic Control of Recombination in Organic Photovoltaics. *Nature* **2013**, *500* (7463), 435−439.
(40) Tamai, Y.; Fan, Y.; Kim, V. O.; Ziabrev, K.; Rao, A.; Barlow, S.; Marder, S. R.; Friend, R. H.; Menke, S. M. Ultrafast Long-Range Charge Separation in Nonfullerene Organic Solar Cells. *ACS Nano* **2017**, *11* (12), 12473−12481.
(41) Gelinas, S.; Rao, A.; Kumar, A.; Smith, S. L.; Chin, A. W.; Clark, J.; Van Der Poll, T. S.; Bazan, G. C.; Friend, R. H. Ultrafast Long-Range Charge Separation in Organic Semiconductor Photovoltaic Diodes. *Opt. InfoBase Conf. Pap.* **2014**, *343*, 512−517.
(42) Ge, Y.; Li, X.; Zhou, M.; Lu, P.; Hao, X. Secondary Aggregation Induced by Volatile Additive for Improved Exciton Diffusion and Charge Separation in High Efficiency Organic Photovoltaic Devices. *Chin. J. Chem.* **2024**, *42*, 2825−2832.
(43) De Sa Pereira, D.; Menelaou, C.; Danos, A.; Marian, C.; Monkman, A. P. Electroabsorption Spectroscopy as a Tool for Probing Charge Transfer and State Mixing in Thermally Activated Delayed Fluorescence Emitters. *J. Phys. Chem. Lett.* **2019**, *10* (12), 3205−3211.
(44) Zhao, Q.; Lai, H.; Chen, H.; Li, H.; He, F. H- And J-Aggregation Inspiring Efficient Solar Conversion. *J. Mater. Chem. A* **2021**, *9* (2), 1119−1126.
(45) Ye, L.; Weng, K.; Xu, J.; Du, X.; Chandrabose, S.; Chen, K.; Zhou, J.; Han, G.; Tan, S.; Xie, Z.; Yi, Y.; Li, N.; Liu, F.; Hodgkiss, J. M.; Brabec, C. J.; Sun, Y. Unraveling the Influence of Non-Fullerene Acceptor Molecular Packing on Photovoltaic Performance of Organic Solar Cells. *Nat. Commun.* **2020**, *11*, No. 6005.
(46) Zhan, L.; Li, S.; Li, Y.; Sun, R.; Min, J.; Bi, Z.; Ma, W.; Chen, Z.; Zhou, G.; Zhu, H.; Shi, M.; Zuo, L.; Chen, H. Desired Open-Circuit Voltage Increase Enables Efficiencies Approaching 19% in Symmetric-Asymmetric Molecule Ternary Organic Photovoltaics. *Joule* **2022**, *6* (3), 662−675.
(47) Mondelli, P.; Kaienburg, P.; Silvestri, F.; Scatena, R.; Welton, C.; Grandjean, M.; Lemaur, V.; Solano, E.; Nyman, M.; Horton, P. N.; Coles, S. J.; Barrena, E.; Riede, M.; Radaelli, P.; Beljonne, D.; Reddy, G. N. M.; Morse, G. Understanding the Role of Non-Fullerene Acceptor Crystallinity in the Charge Transport Properties and Performance of Organic Solar Cells. *J. Mater. Chem. A* **2023**, *11* (30), 16263−16278.
(48) He, C.; Chen, Z.; Wang, T.; Shen, Z.; Li, Y.; Zhou, J.; Yu, J.; Fang, H.; Li, Y.; Li, S.; Lu, X.; Ma, W.; Gao, F.; Xie, Z.; Coropceanu, V.; Zhu, H.; Bredas, J. L.; Zuo, L.; Chen, H. Asymmetric Electron Acceptor Enables Highly Luminescent Organic Solar Cells with Certified Efficiency over 18%. *Nat. Commun.* **2022**, *13*, No. 2598.
(49) Karuthedath, S.; Gorenflot, J.; Firdaus, Y.; Chaturvedi, N.; De Castro, C. S. P.; Harrison, G. T.; Khan, J. I.; Markina, A.; Balawi, A. H.; Peña, T. A. D.; Liu, W.; Liang, R.-Z.; Sharma, A.; Paleti, S. H. K.; Zhang, W.; Lin, Y.; Alarousu, E.; Lopatin, S.; Anjum, D. H.; Beaujuge, P. M.; De Wolf, S.; McCulloch, I.; Anthopoulos, T. D.; Baran, D.; Andrienko, D.; Laquai, F. Intrinsic Efficiency Limits in Low-Bandgap Non-Fullerene Acceptor Organic Solar Cells. *Nat. Mater.* **2021**, *20*, 378−384.

https://doi.org/10.1021/acs.jpclett.5c02643
J. Phys. Chem. Lett. 2025, 16, 10703−10711